Biosensors and Bioelectronics 26 (2011) 2413–2418

Contents lists available at ScienceDirect

Biosensors and Bioelectronics

journal homepage: www.elsevier.com/locate/bios

Label free sub-picomole level DNA detection with Ag nanoparticle decorated Au nanotip arrays as surface enhanced Raman spectroscopy platform

Hung-Chun Lo[a], Hsin-I Hsiung[b], Surojit Chattopadhyay[c,*], Hsieh-Cheng Han[b], Chia-Fu Chen[d,**], Jih Perng Leu[a], Kuei-Hsien Chen[b,e], Li-Chyong Chen[b,***]

[a] Department of Materials Science and Engineering, National Chiao-Tung University, Hsinchu 300, Taiwan
[b] Center for Condensed Matter Sciences, National Taiwan University, Taipei 106, Taiwan
[c] Institute of Biophotonics, National Yang-Ming University, 155, sec-2, Li-Nong Street, Taipei 112, Taiwan
[d] Department of Materials Science and Engineering, Ming-Dao University, Changhua 523, Taiwan
[e] Institute of Atomic and Molecular Sciences, Academia Sinica, Taipei 106, Taiwan

ARTICLE INFO

Article history:
Received 6 September 2010
Accepted 11 October 2010
Available online 16 October 2010

Keywords:
Biosensor
Surface enhanced Raman spectroscopy
DNA
Surface plasmon
Nanostructure

ABSTRACT

Label free optical sensing of adenine and thymine oligonucleotides has been achieved at the sub-picomole level using self assembled silver nanoparticles (AgNPs) decorated gold nanotip (AuNT) arrays. The platform consisting of the AuNTs not only aids in efficient bio-immobilization, but also packs AgNPs in a three dimensional high surface area workspace, assisting in surface enhanced Raman scattering (SERS). The use of sub-10 nm AgNPs with optimum inter-particle distance ensures amplification of the chemically specific Raman signals of the adsorbed adenine, thymine, cytosine and guanine molecules in SERS experiments. High temporal stability of the Raman signals ensured reliable and repeatable DNA detection even after three weeks of ambient desk-top conservation. This facile architecture, being three dimensional and non-lithographic, differs from conventional SERS platforms.

1. Introduction

Surface enhanced Raman scattering (SERS) has developed into a frontline tool for chemical analysis and sensing (Aroca, 2006), since its discovery (Fleischmann et al., 1974), owing to an improved scattering cross-section over the conventional spontaneous Raman process and its efficacy at room temperatures. The enhancement of the Raman scattering cross-section (>10^6) is believed to be due to a surface plasmon aided stronger electro magnetic coupling at the analyte site (Moskovits, 1985; Nie and Emory, 1997). However, another school of thought attributes the enhancement to a chemical charge transfer effect, though it could only predict a theoretical enhancement of the Raman scattering cross-section to the tune of 10^2 (Moskovits, 1985). Apart from the range of organic and inorganic molecules successfully detected using SERS, the technique is becoming increasingly important for bio-sensing (Tripp et al., 2008; Vo-Dinh et al., 2010). Fodor et al. (1985) used a pulsed ultraviolet (UV) laser to enhance the signals from the mononucleotide of adenine (A), thymine (T), cytosine (C) and guanine (G) with limited success. Silver nanoparticle (AgNP) aided SERS was well established for the detection of the nonfluorescent bio-species, such as DNA and fluorescent biomarkers (Brolo et al., 2004; Faulds et al., 2004, 2005; Kneipp et al., 1997; Krug et al., 1999; Stokes et al., 2007; Sun et al., 2007; Wei and Xu, 2007; Zhang et al., 2005). However, Ag did not participate as well as Au in bio-immobilization. For this purpose, gold (Au) plays a major role in establishing the Au–S (gold–sulphur) bond to efficiently immobilize the thiolated bio-species on the substrate, but lost out on the enhancement, and hence sensitivity, of the SERS process against Ag. Conventional detection techniques, such as fluorescence, yielded detection limits of 10^{-13} M from dye labeled-DNA sequences dispersed in AgNP containing buffer solution (Faulds et al., 2004, 2005; Kneipp et al., 1997; Zhang et al., 2005). However, those are indirect detection schemes in the solution phase. The use of Au nanostructures to obtain high immobilization was also employed to detect labeled-DNA sequences through SERS (Brolo et al., 2004; Krug et al., 1999; Stokes et al., 2007; Sun et al., 2007). These detection schemes were limited by the complex sample preparation and relatively low enhancement factors compared to AgNP, as discussed before (Stokes et al., 2007). For increased reliability, measurements using solid substrates were also reported (Brolo et al., 2004; Wei and Xu, 2007).

A recent development, tip enhanced Raman spectroscopy (TERS), has demonstrated detection of low concentration non-fluorescent analytes such as DNA (Becker et al., 2008; Domke et al.,

* Corresponding author. Tel.: +886 2 28267909; fax: +886 2 28235460.
** Corresponding author. Tel.: +886 4 8876660x1030.
*** Corresponding author. Tel.: +886 2 33665249; fax: +886 2 23655404.
E-mail addresses: sur@ym.edu.tw, suroch@gmail.com (S. Chattopadhyay), cfchen@mdu.edu.tw (C.-F. Chen), chenlc@ntu.edu.tw (L.-C. Chen).

0956-5663/$ – see front matter © 2010 Elsevier B.V. All rights reserved.
doi:10.1016/j.bios.2010.10.022

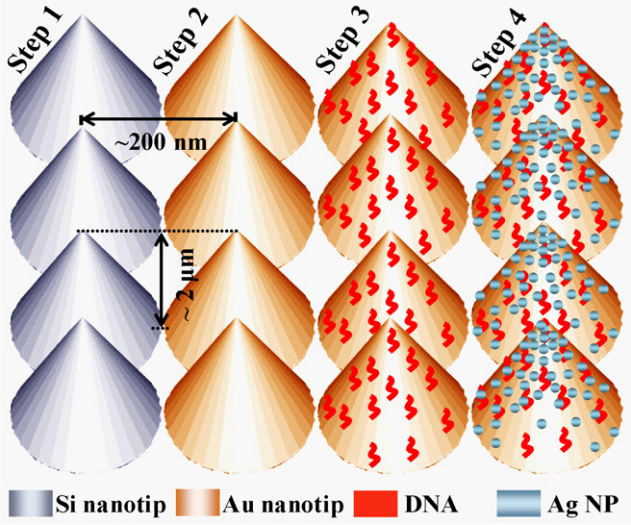

Fig. 1. A schematic of the pathway for generating the SERS platform. Step 1: the as-grown silicon nanotip array template; Step 2: Au coating of the SiNT array to generate the AuNT array for efficient DNA immobilization; Step 3: immobilization of DNA molecules on the AuNT array; Step 4: silver nanoparticle (AgNP) deposition for efficient Raman signal enhancement.

2007; Ichimura et al., 2007; Rasmussen and Deckert, 2006) and fluorescent biomarkers (Domke et al., 2006). This near-field technique, an emerging competitor of SERS for detection purposes, demonstrated significantly high spatial resolution and sensitivity by tuning the gap between the apex of the cantilever tip and the substrate. However, challenges, such as fabricating uniform TERS tips, nano-scale heating and mismatch between topography and optical signal, remain for the development of this technique (Yeo et al., 2009). Being excellent otherwise, TERS can also be prohibitively expensive and complicated for routine measurements compared to SERS.

We demonstrate here a simple SERS platform that uses AgNP decorated Au nanotips (AuNTs) array that incorporates the immobilization efficiency of Au and enhanced Raman scattering efficiency of the AgNPs (Fig. 1) for label-free, high-sensitivity DNA detection. In addition, we demonstrate high and tunable three dimensional packing densities of the AgNPs that could maximize the SERS enhancement and increase its stability.

2. Materials and methods

2.1. SERS substrate preparation

In this study, a semiconductor compatible electron cyclotron resonance microwave plasma enhanced chemical vapor deposition (ECR-MWPECVD) and an ion beam sputtering deposition (IBSD) system was used to fabricate the silicon nanotip (SiNT) arrays and the Au/Ag coated nanostructure, respectively. The high density ECR plasma of silane (SiH_4), methane (CH_4), hydrogen (H_2) and argon (Ar) gas mixture was used to fabricate (top down process) the well aligned SiNTs from commercial 6 inch single crystalline silicon wafers (Fig. 1, step 1). The detailed description of the SiNT formation is published elsewhere (Chattopadhyay et al., 2006; Hsu et al., 2004; Lo et al., 2003). The IBSD technique used a Kaufman type ion source and its application to the deposition of noble metals (bottom up process) could be found elsewhere (Chattopadhyay et al., 2005a,b). As shown later, surface modification of the SiNTs *via* an Au thin film (Fig. 1, step 2) aids in high efficiency DNA immobilization (Fig. 1, step 3), and subsequent deposition of AgNPs (Fig. 1, step 4) ensures superior sensitivity Raman measurement.

2.2. DNA immobilization

The AuNT substrates were incubated with single strand (*ss*) probes (*p*-DNA) for 24 h at 4 °C for immobilization (Fig. 1, step 3). Thiol-modified *p*-DNA (MDBio) with a 20-base sequence, 5′-HS-$(CH_2)_6$-AAAAAAAAAAAAAAAAAAAA-3′, was diluted to 10 mM with 2× saline sodium citrate (SSC) buffer. Before hybridization procedure, Cleland's Reductacryl reagent (EMD Biosciences) was added to prevent the aggregation of the *p*-DNA and the mixture, of *p*-DNA and reducing agent, was then filtered *via* MicroSpinTH G25 column (GE Healthcare) at 3000 rpm for 2 min. A specific 20-base *ss*-oligonucleotide, 5′-TTTTTTTTTTTTTTTTTTTT-3′, complementary to the *p*-DNA, was selected as the target (*t*-DNA). Duplex buffer solution (Integrated DNA Tech.) was further added to reach a final concentration of 10 mM, prior to hybridization studies. After each of the above-mentioned steps, the sample was washed carefully in de-ionized water, followed by drying in nitrogen flow, in order to avoid the physisorption (or non-specific binding) of chemicals in solution or *p*-DNA on the AuNTs surface. Similar technique was adopted for the *ss*-C and G nucleotides. No fluorescent labels or Raman dyes were used.

2.3. Analyses

High resolution field emission scanning electron microscope (JEOL JSM-6700 FESEM) was used to study the structure and morphology of the bare SiNTs, AuNTs and the AgNPs density distribution. Raman spectroscopy measurements were carried out in a Jobin Yvon LabRAM HR800 micro Raman spectroscope system. A 632 nm He–Ne laser (beam diameter ~1.5 μm) with a power density of 4.5 mW/μm^2 and acquisition time of 60 s was used.

3. Results and discussion

3.1. Morphology and architecture of the nanotip based SERS platform

In this study, a top-down self-masked dry etching (SMDE) technique was developed to create the SiNTs template (Fig. 1, step 1) over a large area (~28 sq. inch) at 200 °C process temperature (Hsu et al., 2004; Lo et al., 2003). These SiNTs had apex diameters typically in the range of ~2–5 nm, bottom diameters of 100–200 nm, aspect ratio around 10–12 (using base diameter of 100 nm) and tip density of 10^{11} cm^{-2}. Conformal Au coating, by IBSD, of these SiNTs resulted in the AuNT array that closely resembled the features of the SiNT template (Fig. 1, step 2). Post DNA immobilization, controlled sputtering of Ag, on these AuNTs, resulted in the bottom-up growth of self assembled AgNPs (Fig. 1, step 4) whose number density, or their average inter-particle distances, could be easily controlled as a function of the sputtering time. Fig. 2 shows the SEM images of plain SiNTs (Fig. 2a), Au thin film coated AuNTs (Fig. 2b and c), and AgNPs decorated AuNTs (Fig. 2d–f). Direct DNA immobilization on AgNP decorated SiNTs (without the Au thin film) was found unsuitable since a fraction of the physisorbed AgNPs along with the DNA strand would be washed away during sample preparation yielding lower Raman signals. Compared with the other cylindrical 1-D nanostructures, the well aligned AuNTs template supports the NP loading without any shadow effect due to its conical morphology, just like its underlying SiNTs template (Chattopadhyay et al., 2005b, 2006). Fig. 2b depicts the well aligned AuNTs with high uniformity, aspect ratio and density. Assuming all the nanotips touching each other at the bottom, the real surface area can be quantified to be around 225 m^2 cm^{-3} (Wenzel, 1949), which is as good as high-porosity porous silicon (Chan et al., 2003; Lo et al., 2006).

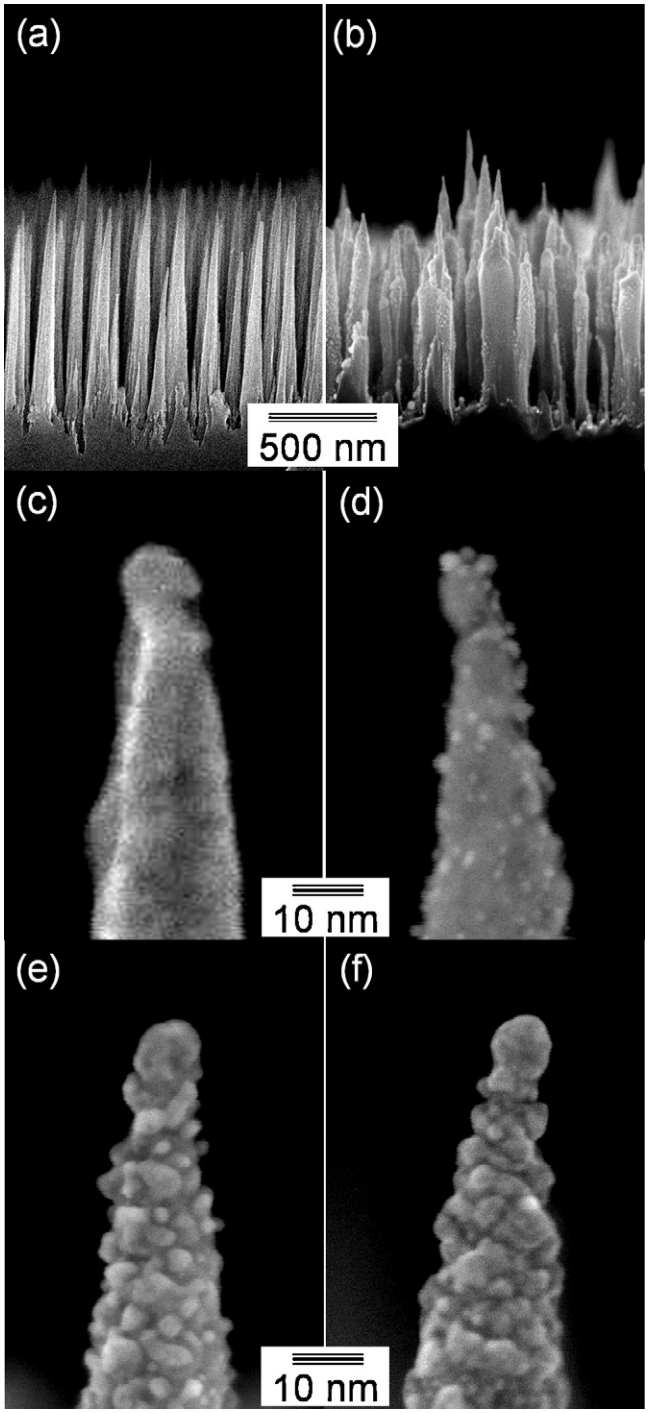

Fig. 2. Cross-section high resolution scanning electron microscopy (SEM) images of (a) as-grown SiNTs, (b) low magnification of Au coated SiNTs, (c) high magnification of Au coated SiNTs; cross-section SEM images of AuNTs covered with AgNPs sputtered for (d) 5, (e) 10 and (f) 20 min by IBSD system.

IBS deposition of Au for 60 min at room temperature on the SiNTs yielded the AuNTs (Fig. 2b and c). Comparing the bare and Au-coated SiNTs, the thickness of the Au layer was estimated to be around ~10 nm at the apex. The thiolated DNA species were then immobilized onto the AuNTs surface followed by the AgNPs deposition. The density of AgNPs, produced on the AuNTs, corresponding to Ag sputtering times of 5, 10 and 20 min are shown in Fig. 2d–f, respectively. The size of these NPs varied between 3 and 10 nm in diameter. For sputtering times of 5 min and above, the AgNPs developed throughout the entire surface of the AuNTs (Fig. 2d).

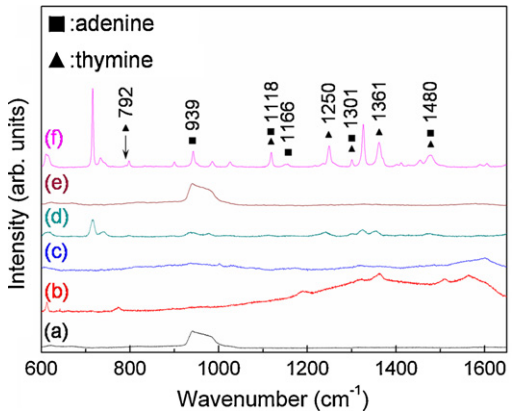

Fig. 3. Raman scattering spectrum of 1.2 nM of (a) Rhodamine 6G adsorbed on SiNT and SERS spectrum of (b) Rhodamine 6G adsorbed on AuNTs. SERS spectrum of hybridized A and T, on AuNT, at (c) 1.2 nM and (d) 12 mM concentrations. (e) Raman spectrum of hybridized *ds*-A + T (12 mM concentration) on planar Si. (f) The Raman spectrum of bulk A and T powder dispersed on planar silicon wafer. The symbols ■ and▲ represent Raman bands of adenine and thymine, respectively.

High density, with 1–2 nm inter-particle distance, and uniformly dispersed AgNPs were observed at an optimized sputtering time of 10 min (Fig. 2e). Longer sputtering times, say 20 min, resulted in agglomerated clusters leading to the formation of an Ag thin film on the AuNTs (Fig. 2f).

3.2. SERS measurement on AuNTs

We began, by studying the SERS activity of the AuNTs vis-à-vis the bare SiNTs. We used a standard analyte, Rhodamine 6G (R6G), with a concentration of 1.2 nM on SiNTs and AuNTs and various concentrations of adenine and thymine on AuNT for this purpose (Fig. 3). The results indicate that R6G absorbed on SiNTs yielded no Raman bands for the analyte (Fig. 3a). The second order Raman band for Si (at 980 cm^{-1}) dominates the spectrum. In contrast, the AuNTs shows finger print R6G Raman bands at ~610, 780, and ~1600 cm^{-1} (Fig. 3b). This indicates that the AuNTs are SERS active, at least for R6G which has a Raman scattering cross-section between ~10^{-30} and 10^{-22} cm^2/mol (Meyer et al., 2010; Nie and Emory, 1997; Shim et al., 2008). However, lower concentrations (1.2 nM) of DNA could not be detected on the AuNTs (Fig. 3c). In contrast, at a higher concentration (1.2×10^{-2} M) rich Raman signals from DNA (adenine and thymine mononucleotide) could be observed from the AuNTs (Fig. 3d). Similar DNA dispersion on bare silicon wafers did not yield any Raman signals (Fig. 3e). This does show limited SERS activity of the AuNTs. In comparison to Fig. 3d, measured at 12 mM, bulk DNA powders dispersed on silicon showed strong and rich Raman signals (Fig. 3f). However, Fig. 3d–f cannot be compared to obtain a SERS enhancement factor since, among other reasons (Le Ru et al., 2007), the non-SERS cross-section of the DNA used is unknown. The results in Fig. 3d–f indicate that either (i) the DNA molecules have significantly lower Raman scattering cross-section than R6G, and/or (ii) the surface plasmon in the AuNTs is too weak to excite the Raman signals from the DNA. The first proposition is reasonable since R6G is a laser dye with strong Raman scattering cross-section (Meyer et al., 2010; Shim et al., 2008). The second proposition is also reasonable since the polarizability, and hence the surface plasmon generation, is weaker in the metal thin films than the rough nanostructured counterparts. Since Au is indispensable for DNA immobilization, an extension of the substrate design was necessary to observe any reliable detection of DNA species through Raman spectroscopy. Accordingly, the additional AgNP decoration of the AuNT was employed to induce a stronger enhancement of the SERS signal from the DNA.

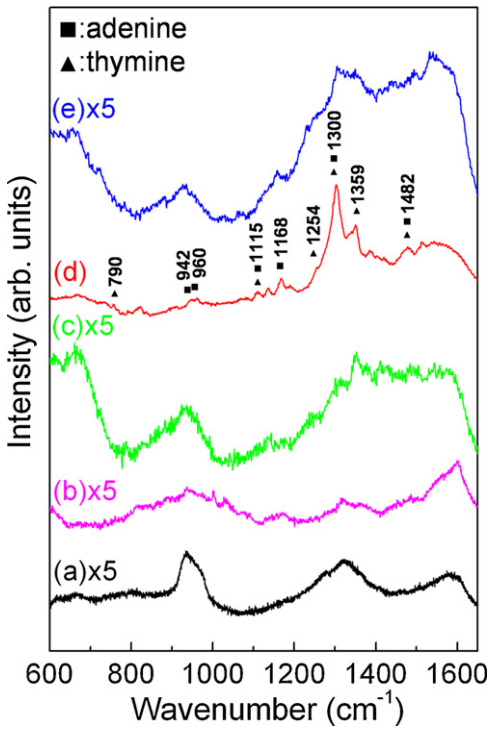

Fig. 4. Raman scattering spectrum of the (a) as-grown AuNTs. SERS spectra of thiolated *ss*-A hybrized with *ss*-T (1.2 nM each) obtained on AuNTs decorated with AgNPs sputtered for (b) 0 (bare AuNTs), (c) 5, (d) 10 and (e) 20 min. The symbols ■ and ▲ represent Raman bands of adenine and thymine, respectively.

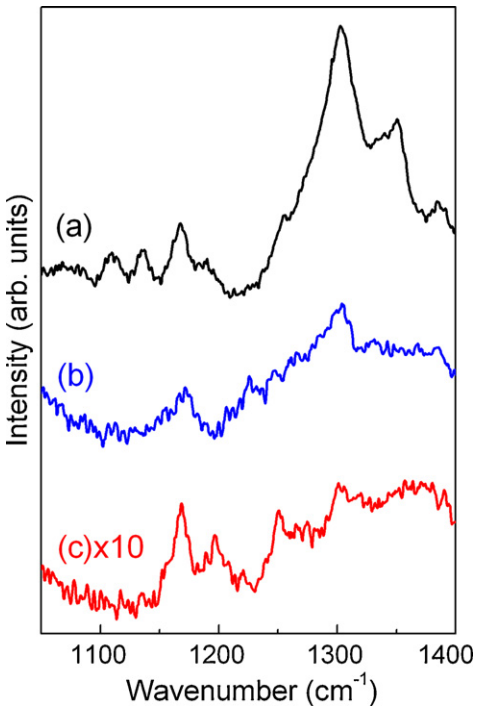

Fig. 5. SERS spectra of thiolated *ss*-A hybrized with *ss*-T, on the optimized substrates (as in Fig. 2e), with concentrations of (a) 1.2 nM, (b) 12 pM and (c) 120 fM.

3.3. SERS measurement on AgNP decorated AuNTs

Raman spectrum from the bare AuNTs (Fig. 4a) and SERS spectra from the DNA immobilized AuNTs (Fig. 4b) were compared with those having different amounts of AgNPs deposited on the DNA molecules (Fig. 4c–e). SERS signals of poly (A) and poly (T) sequences with 1.2 nM concentration were reliably detected only from the AgNPs coated AuNTs (Fig. 4c–e). DNA Raman signals from AuNTs (Ag coating time of 0 min, Fig. 4b) showed no reproducible Raman signals. This clearly demonstrates the contribution from the AgNPs.

Weak DNA Raman signals, from the 5 and 20 min grown AgNPs (as in Fig. 2d and f, respectively), appeared mostly within 700–1650 cm^{-1} (Fig. 4c and e). The assignment of the peaks to the vibration modes of A and T is indicated in Fig. 4d (Domke et al., 2007; Fodor et al., 1985; Ichimura et al., 2007; Rasmussen and Deckert, 2006). Enhanced SERS signal of the DNA chains (Fig. 4d) could only be obtained from the 10 min grown AgNPs which are uniformly dispersed and have higher density (Fig. 2e) compared to others shown in Fig. 2. The peaks, in the SERS spectra of the *ss*-A and T, are now better resolved and more intense for easy identification and assignment (Fig. 4d) (Domke et al., 2007; Ichimura et al., 2007; Rasmussen and Deckert, 2006). AuNT substrates with Ag films, obtained with longer duration (20 min) sputtering, yielded very weak Raman signals (Fig. 4e). This is attributed to the difficulty in polarizing the Ag thin films, compared to the nanometric Ag particles, and hence a lowering of the surface plasmon strength upon laser irradiation. The suppressed SERS signal in Fig. 4e may also be due to the masking of the DNA molecules underneath the Ag film.

Density of the metal NPs are more critical than its size with regard to cross-section enhancement as pointed out by Garcia-Vidal and Pendry in their calculation (García-Vidal and Pendry, 1996). We refer to their work to explain why the sparse AgNPs (Fig. 2d) or the Ag thin film (Fig. 2f) did not yield high enhancements as in the case of the high density AgNPs (Fig. 2e) (García-Vidal and Pendry, 1996). They predicted that the SERS enhancement will go to a maximum when the central separation, d, between the metallic particles (Ag in this case) is equal to the particle diameter ($2r$), or in other words, when the adjacent AgNPs are touching each other. This is the theoretical recipe for SERS '*hot-spots*' provided by García-Vidal and Pendry (1996), though experimental isolation of a '*hot-spot*' is still illusive. Single molecule detection schemes had to rely on SERS '*hot-spots*' whose enhancement factors were estimated about million times higher than an average SERS active metal site with enhancement factors of 10^6–10^8 (Camden et al., 2008; Kneipp et al., 1997; Michaels et al., 1999; Nie and Emory, 1997). This ideal condition for maximum SERS enhancement, or so-called '*hot-spots*', is close to what we have for the AuNTs covered with AgNPs grown for 10 min (Fig. 2e; $d \sim 2.5r$). This is our optimized SERS platform. Longer Ag deposition time, $d \ll 2r$ or shorter Ag coating times (5 min or less), $d \gg 2r$ dramatically decreased the SERS activity of the metal. Our experimental results are in agreement with their calculations. At this point, it is essential to point out that this technique may not be limited to the A and T nucleotides only, but can well be extended to C, G and their hybridized double strands (*ds*-) also (see Fig. S1 in Supplementary Data).

It is only natural to argue that the above results of DNA detection could also be obtained on a planar Au film instead of the high aspect ratio AuNTs used as the platform. Qualitatively, a similar result is expected before we consider the following facts. AgNPs with ~10 nm size and controllable density could not be grown on Au thin films due to severe agglomeration effect leading to island formation (Kang and Bernstein, 1976). AuNTs, with high roughness, impart a suitable surface energy so that Ag self-assembles as AgNPs, with controllable density and dimension, on it. Modification of the AuNT surface with DNA molecules may add to the effect that helps create the AgNPs. However, even the bare silicon nanotips can self-assemble AgNPs without the help of any DNA coverage (Chattopadhyay et al., 2005b). Secondly, AuNTs, with high surface area, can generate a high packing density of AgNPs in three dimen-

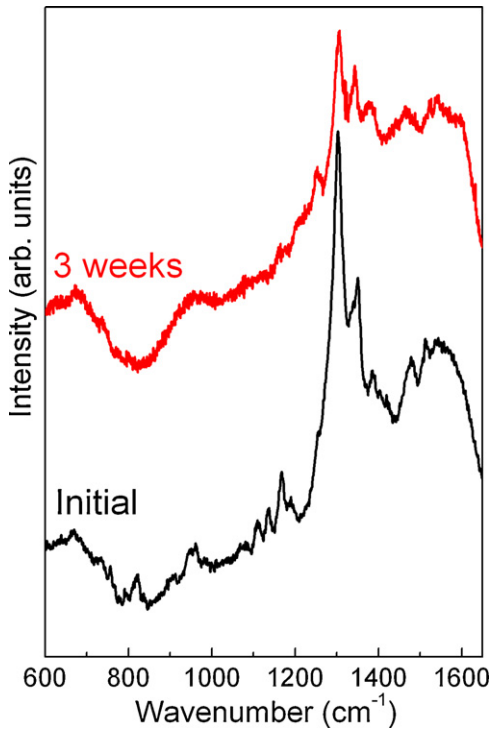

Fig. 6. Time decay of the SERS spectrum. Aging of SERS spectrum of 1.2 nM of hybridized *ds*-A with T on AuNTs decorated with AgNPs sputtered for 10 mins (optimized substrate, as in Fig. 2e).

sions (3D) (see Fig. 1, step 4) instead of a 2D packing of islands obtainable on a thin film. This is a key distinction of this nanotip platform as against the lithographically prepared planar SERS platforms. The 3D packing of the AgNPs ensures that even with the laser tightly focused to ~1.5 μm spot (used in this micro-Raman study), it could actually excite a larger number density of AgNPs and hence achieve a significant SERS signal from the adsorbed analyte. However, the SERS signal of the DNA clearly arises from its electromagnetic interaction with the AgNPs and not due to an increased number density of DNA adsorbed on the rough nanotips. This is because bare AuNTs, with high immobilization efficiency, did not produce any enhanced SERS signal of the DNA (Fig. 3c) compared to Fig. 4d.

Fig. 5 shows the SERS signals from different concentrations of hybridized *ds*-DNA on the optimized AgNPs coated AuNTs (as in Fig. 2e). The high SERS enhancement of the AuNT array based sensing platform enabled DNA detection down to 1.2×10^{-13} M concentration. The 1168 cm^{-1} Raman fingerprint signals of the A and T species and 1300 cm^{-1} of the T species (Domke et al., 2007; Ichimura et al., 2007; Rasmussen and Deckert, 2006) were clearly resolvable at the lowest concentration. The integrated intensity of the 1300 cm^{-1} line of T (see Fig. S3 in Supplementary Data), as a function of concentration, shows a variation similar to what the Langmuir isotherm would predict and is nearly linear over the 120 fM to 10 nM range.

3.4. Stability of the SERS platform (AgNP decorated AuNT arrays)

Lastly, any practical sensor platform must demonstrate a reasonable stability, given the fact that surface enhanced Raman signals are known to decay within hours of preparation. The stability of the current platform was tested by measuring the Raman activity with time. Individual *ss*-DNA, with 10^{-6} M concentrations, immobilized on our optimized platform showed 50–65% remnant intensity (of the strongest Raman line) after 144 h of storage in ambient desk-top conditions (see Fig. S3 in Supplementary Data). The data in Fig. S3 contains a scatter of five similar experiments on different pieces of the same substrate. Hence, the scatter is a measure of the reproducibility of the substrates. Even low concentrations (1.2 nM) of hybridized *ds*-DNA can retain up to ~40% of the initial intensity of a particular Raman line even after 3 weeks of the immobilization when conserved under normal desktop conditions on the optimized substrates (Fig. 6). These results demonstrate outstanding stability characteristics enabling clear and unambiguous detection.

4. Conclusions

In conclusion, a high aspect ratio, three dimensional AuNTs array decorated by AgNPs was used for high-sensitivity label-free DNA detection *via* the surface enhanced Raman scattering (SERS) technique. Sub-picomole DNA concentrations (~10^{-13} M) could be detected in a reproducible and stable manner using this new generation SERS platform. The stability of these substrates could span over few weeks and is possibly due to the high adsorption efficiency of the SERS active sites. The entire process of substrate fabrication is semiconductor process compatible, promoting the possibility of a device fabrication.

Acknowledgments

The authors would like to acknowledge National Science Council, Taiwan and Air Force Office of Scientific Research, USA for financial support.

Appendix A. Supplementary data

Supplementary data associated with this article can be found, in the online version, at doi:10.1016/j.bios.2010.10.022.

References

Aroca, R., 2006. Surface Enhanced Vibrational Spectroscopy. John-Wiley & Sons, Toronto.
Becker, M., Sivakov, V., Gösele, U., Stelzner, T., Andrä, G., Reich, H.J., Hoffmann, S., Michler, J., Christiansen, S.H., 2008. Small 4 (4), 398–404.
Brolo, A.G., Arctander, E., Gordon, R., Leathem, B., Kavanagh, K.L., 2004. Nano Lett. 4 (10), 2015–2018.
Camden, J.P., Dieringer, J.A., Wang, Y., Masiello, D.J., Marks, L.D., Schatz, G.C., Van Duyne, R.P., 2008. J. Am. Chem. Soc. 130 (38), 12616–12617.
Chan, S., Kwon, S., Koo, T.W., Lee, L.P., Berlin, A.A., 2003. Adv. Mater. 15 (19), 1595–1598.
Chattopadhyay, S., Shi, S.C., Lan, Z.H., Chen, C.F., Chen, K.H., Chen, L.C., 2005a. J. Am. Chem. Soc. 127 (9), 2820–2821.
Chattopadhyay, S., Lo, H.C., Hsu, C.H., Chen, L.C., Chen, K.H., 2005b. Chem. Mater. 17 (3), 553–559.
Chattopadhyay, S., Chen, L.C., Chen, K.H., 2006. Crit. Rev. Solid State Mater. Sci. 31 (1 & 2), 15–53.
Domke, K.F., Zhang, D., Pettinger, B., 2006. J. Am. Chem. Soc. 128 (45), 14721–14727.
Domke, K.F., Zhang, D., Pettinger, B., 2007. J. Am. Chem. Soc. 129 (21), 6708–6709.
Faulds, K., Smith, W.E., Graham, D., 2004. Anal. Chem. 76 (2), 412–417.
Faulds, K., Stewart, L., Smith, W.E., Graham, D., 2005. Talanta 67 (3), 667–671.
Fleischmann, M., Hendra, P.J., McQuillan, A.J., 1974. Chem. Phys. Lett. 26 (2), 163–166.
Fodor, S.P.A., Rava, R.P., Hays, T.R., Spiro, T.G., 1985. J. Am. Chem. Soc. 107 (6), 1520–1529.
García-Vidal, F.J., Pendry, J.B., 1996. Phys. Rev. Lett. 77 (6), 1163–1166.
Hsu, C.H., Lo, H.C., Chen, C.F., Wu, C.T., Hwang, J.S., Das, D., Tsai, J., Chen, L.C., Chen, K.H., 2004. Nano Lett. 4 (3), 471–475.
Ichimura, T., Watanabe, H., Morita, Y., Verma, P., Kawata, S., Inouye, Y., 2007. J. Phys. Chem. C 111 (26), 9460–9464.
Kang, S.K., Bernstein, I.M., 1976. Philos. Mag. 33 (4), 709–714.
Kneipp, K., Wang, Y., Kneipp, H., Perelman, L.T., Itzkan, I., Dasari, R.R., Feld, M.S., 1997. Phys. Rev. Lett. 78 (9), 1667–1670.
Krug, J.T., Wang, G.D., Emory, S.R., Nie, S., 1999. J. Am. Chem. Soc. 121 (39), 9208–9214.
Le Ru, E.C., Blackie, E., Meyer, M., Etchegoin, P.G., 2007. J. Phys. Chem. C 111 (37), 13794–13803.
Lo, H.C., Das, D., Hwang, J.S., Chen, K.H., Hsu, C.H., Chen, C.F., Chen, L.C., 2003. Appl. Phys. Lett. 83 (7), 1420–1422.

Lo, H.C., Huang, Y.F., Chattopadhyay, S., Hsu, C.H., Chen, C.F., Chen, K.H., Chen, L.C., 2006. Nanotechnology 17 (10), 2542–2545.
Meyer, S.A., Le Ru, E.C., Etchegoin, P.G., 2010. J. Phys. Chem. A 114 (17), 5515–5519.
Michaels, A.M., Nirmal, M., Brus, L.E., 1999. J. Am. Chem. Soc. 121 (43), 9932–9939.
Moskovits, M., 1985. Rev. Mod. Phys. 57 (3), 783–826.
Nie, S., Emory, S.R., 1997. Science 275 (5303), 1102–1106.
Rasmussen, A., Deckert, V., 2006. J. Raman Spectrosc. 37 (1), 311–317.
Shim, S., Stuart, C.M., Mathies, R.A., 2008. Chem. Phys. Chem. 9 (5), 697–699.
Stokes, R.J., Macaskill, A., Lundahl, P.J., Smith, W.E., Faulds, K., Graham, D., 2007. Small 3 (9), 1593–1601.
Sun, L., Yu, C., Irudayaraj, J., 2007. Anal. Chem. 79 (11), 3981–3988.
Tripp, R.A., Dluhy, R.A., Zhao, Y., 2008. Nano Today 3 (3–4), 31–37.
Vo-Dinh, T., Wang, H.N., Scaffidi, J., 2010. J. Biophoton. 3 (1–2), 89–102.
Wei, H., Xu, H., 2007. Appl. Phys. A 89 (2), 273–275.
Wenzel, R.N., 1949. J. Phys. Chem. 53 (9), 1466–1467.
Yeo, B.S., Stadler, J., Schmid, T., Zenobi, R., Zhang, W., 2009. Chem. Phys. Lett. 472 (1–3), 1–13.
Zhang, X., Young, M.A., Lyandres, O., Duyne, R.P.V., 2005. J. Am. Chem. Soc. 127 (12), 4484–4489.